Mass-fabrication scheme of highly sensitive wireless electrodeless MEMS QCM biosensor with antennas on inner walls of microchannel

Lianjie Zhou,[†,⊥] Fumihito Kato,[‡,⊥] Masumi Iijima,[¶] Tomoyuki Nonaka,[§] Shun'ichi Kuroda,[‖] and Hirotsugu Ogi[*,†]

†*Graduate School of Engineering, Osaka University, Yamadaoka 2-1, Suita, Osaka 565-0871, Japan*

‡*Department of Mechanical Engineering, Nippon Institute of Technology, Gakuendai 4-1, Miyashiro-machi, Minamisaitama, Saitama 345-8501, Japan*

¶*Department of Nutritional Science and Food Safety, Tokyo University of Agriculture, Sakuragaoka 1-1-1, Setagaya-ku, Tokyo 156-8502, Japan*

§*Samco Inc., Waraya-cho 36, Takeda, Fushimi-ku, Kyoto 612-8443, Japan*

‖*SANKEN, Osaka University, Mihogaoka 8-1, Ibaraki, Osaka 567-0047, Japan*

⊥*Contributed equally to this work*

E-mail: ogi@prec.eng.osaka-u.ac.jp

Phone: +81-6-6879-7276. Fax: +81-6-6879-7276

Abstract

Quartz-crystal-microbalance (QCM) biosensor is a typical label-free biosensor, and its sensitivity can be greatly improved by removing electrodes and wires that would be otherwise attached to the surfaces of the quartz resonator. The wireless-electrodeless QCM biosensor was then developed using a micro-electro-mechanical systems (MEMS)

process, although challenges remain in the sensitivity, the coupling efficiency, and the miniaturization (or mass production). In this study, we establish a MEMS process to obtain a large number of identical ultra-sensitive and highly efficient sensor chips with dimensions of 6 mm square. The fundamental shear resonance frequency of the thinned AT-cut quartz resonator packaged in the microchannel exceeds 160 MHz, which is excited by antennas deposited on inner walls of the microchannel, significantly improving the electro-mechanical coupling efficiency in the wireless operation. The high sensitivity of the developed MEMS QCM biosensors is confirmed by the immunoglobulin G (IgG) detection using protein A and ZZ-tag displaying bio-nanocapsule (ZZ-BNC), where we find that the ZZ-BNC can provide more effective binding sites and higher affinity to the target molecules, indicating a further enhancement in the sensitivity of the MEMS QCM biosensor. We then perform the label-free C-reactive protein (CRP) detection using the ZZ-BNC functionalized MEMS QCM biosensor, which achieves the detection limit of 1 ng·mL^{-1} or less even with the direct detection.

INTRODUCTION

Highly sensitive and reliable biosensors are crucial in diagnosis, environmental monitoring, and drug discovery.[1] Among various biosensors, the reverse transcription-polymerase chain reaction (RT-PCR) test and the enzyme-linked immunosorbent assay (ELISA) have highly contributed to gaining control of the COVID-19 pandemic, although they suffer from inadequacy in assay sensitivity.[2–4] Surface-plasmon-resonance (SPR) biosensor is another representative and advanced method that allows the label-free detection.[5–7] However, the expensive equipments and complex sensing system limit the point-of-care application.[8] On the other hand, quartz-crystal-microbalance (QCM) sensors have important advantages, including simple and compact instrumentation, low-cost, high stability, and capability for real-time monitoring, and they have been widely used as force sensors,[9] humidity sensors,[10,11] gas sensors,[12–14] and biosensors.[15–17] The QCM biosensor detects target biomolecules mainly

through the mass loading effect, which is measured from a decrease in the resonance frequency.[18] The conventional QCM sensor consists of a quartz plate (or resonator) with electrodes on both sides to which wires are connected. The electrodes cause significant inertia resistance at the resonator surfaces due to much larger mass density than that of quartz, deteriorating the mass sensitivity of QCM.[19,20] In addition, electric connectors on the quartz resonator for fixation, power supply, and signal detection not only deteriorate the quality factor of the resonator but also limit the use of a resonator with high fundamental resonant frequency ($<\sim$10 MHz).[21–23] To improve the operating frequency and thus the sensitivity of QCM, the wireless and electrodeless QCM has been developed using the micro-electro-mechanical-systems (MEMS) processes.[24–26] Instead of using the contacting electrodes, excitation and detection of the shear vibration are achieved by non-contacting antennas in the wireless QCM. Although Au films were occasionally used for forming a self-assembled monolayer through the alkanethiol reaction, their thickness was only several nanometers, affecting little QCM's mass sensitivity. This wireless and non-fixation manner allows the use of extremely thin and high-frequency resonators, thus significantly improving the sensitivity of the QCM biosensor.[27]

The reliable and accurate detection of biomarkers with low concentrations or small molecules remains challenging. For a QCM biosensor, the frequency shift is proportional to the additional mass loading on its surface. Therefore, various mass-amplification methods have been proposed to improve the mass sensitivity of the QCM biosensor. For example, alternative receptors modified by heavy materials such as micro/nanobeads,[28] gold nanoparticles (AuNPs),[29–31] streptavidin,[32,33] and ZZ-tag displaying bio-nanocapsule (ZZ-BNC)[34] have been used to enhance the frequency change through their binding with target molecules. Compared with these sandwich mass amplification methods, which take longer assay time because of extra incubation and washing procedures, a direct method is preferable by improving the binding efficiency of receptors to target molecules either by increasing the area density of receptors[35,36] or by regulating the orientation of receptors.[21,37,38] Oriented

immobilization of antibody molecules with their antigen-binding fragments (Fab) away from the sensor surface can increase the effective binding sites, and thus the sensor response. This immobilization strategy has been accomplished by priorly immobilizing an intermediate scaffold (for example, protein A or protein G) on the sensor surface, which binds to the constant fragment (Fc) region of the antibodies.[39–42] However, it is difficult to fully control their orientation.[43] The scaffolds for orientation fixation should be both rigid to avoid the steric hindrance and flexible to capture target molecules approaching from various directions, which has been difficult to achieve with conventional scaffolds. We previously developed ZZ-BNC with a lipid bilayer membrane and envelope L proteins.[44] The L protein is modified by replacing its N-terminal region with a protein A-derived IgG Fc-binding Z domain.[45] The ZZ-BNC can enhance the sensitivity of immunosensors through not only the oriented immobilization but also the clustering of antibodies. It also possesses the moderate flexibility for target capturing.[46,47] Furthermore, the ZZ-BNC is stable to heat, chemical, and mechanical stress,[48] thus can be used as a practical scaffold for oriented immobilization.

Good signal strength and quality factor are required in QCM biosensors, especially in detecting low-concentration targets, because they determine the minimum measurable frequency shift. However, in the wireless QCM, the signal strength decreases with thinning the resonator because of the trade-off with the non-contacting measurement. We previously developed a wireless MEMS QCM biosensor, where the excitation of quartz resonator and signal readout are performed by the antennas outside the sensor chip.[24] The long fluid microchannel resulted in a large sensor chip with 20-mm[24,49] or 10-mm[26] length. The relatively long distance between the quartz resonator and the antennas deteriorates the signal-to-noise ratio.

In this paper, we present a compact wireless MEMS QCM biosensor, in which the antennas are deposited on the inner walls of the microfluidic channel. Innovatively, we embedded metallic micropillars through the glass substrates to activate the inner antennas from the outside conduction layers, resulting in significant enhancement in the signal strength because

of the shortened distance between the resonator and antennas. This configuration allows us to use an extremely thin quartz resonator with the fundamental frequency of up to 166 MHz, the highest frequency among reported MEMS QCM sensors. In this study, we have established a MEMS process that allows fabrication of the MEMS QCMs with this special structure in a small size and in large quantities. We confirm its high sensitivity with IgG and C-reactive-protein (CRP) detection assays despite the smallest size. Furthermore, we find that our previously proposed ZZ-BNC can provide more binding sites and higher binding affinity to IgG than the randomly immobilized protein A.

MATERIALS AND METHODS

Fabrication of Sensor Chips

Figure S1 in Supporting Information summarizes the wafer-scale MEMS process proposed in this study. It principally consists of four processes: (i) Glass-wafer process for fabricating upper and bottom glass wafers with microchannels and inner and outer antennas. (ii) Silicon-on-insulator (SOI) wafer process for making the middle Si layer as the bonding layer. (iii) Quartz-wafer process for patterning the isolated thin quartz resonators. And (iv) packaging process. Briefly, we first prepared two glass wafers with through-tungsten micropillars and processed them for fabricating microchannels. We then deposited antennas on the inner and outer surfaces, which are electrically connected by the tungsten micropillars. The SOI wafer was processed by the plasma-reactive ion-etching (ICP-RIE) method for removing Si in the microchannel parts and bonded to one of the processed glass wafers by the anodic bonding method. Then, the thicker Si substrate layer was removed by the ICP-RIE method, and the insulator (SiO_2) layer was removed by cleaning with hydrofluoric acid. (The remaining Si portion serves as the bonding layer to the other glass wafer.) In the quartz-wafer process, an AT-cut quartz wafer was bonded to a Si wafer by diffusion bonding, mechanically polished, and processed via an etching gas for making thin resonators. The sacrificial

dots for bonding were made at the resonator surface sites that coincide with the tip of the tungsten pillar, through which the other glass wafer was bonded. By removing the Si wafer, the very thin quartz resonators were fixed inside the microchannels of the glass wafer by the sacrificial bonding dots on the tungsten micropillars. Finally, using the anodic bonding method, the quartz resonators were packaged, and by flowing a specific solution (an alkali solution including tetramethylammonium hydroxide) inside the microchannels for dissolving the sacrificial dots, many ($>\sim 180$) highly sensitive MEMS QCM chips were obtained. The detailed structure of a single chip is shown in Fig. 1. In the MEMS-QCM chip fabricated in this way, the quartz resonator is placed in the microchannel without any fixing parts; it is lightly supported by the tungsten micropillars and Si semicircular walls. At the start of the measurement, a slight in-plane movement of the quartz plate is expected due to the solution flow, but this is immediately restricted by the semicircular walls of Si, giving insignificant effect on the frequency stability.[24]

MEMS QCM Functionalization for IgG Detection

The QCM functionalization process for IgG detection using protein A is similar to that in our previous study.[26] First, we rinsed the MEMS QCM biosensor by injecting piranha solution (98% H_2SO_4:30% H_2O_2 =7:3) and ultrapure water into the microchannel of the sensor chip using a pipette. We then injected the 10 mM self-assembled monolayer (SAM) molecules in absolute ethanol and incubated the sensor chip overnight at 4 °C to immobilize the linkers. The SAM molecules were then activated by injecting a mixture of 100 mM N-hydroxysulfosuccinimide sodium salt (NHS) and 100 mM 1-ethyl-3-(3-dimethylaminopropyl) carbodiimide hydrochloride (EDC) and incubating at room temperature for 1 hour. After the activation procedure, 200 μg·mL^{-1} Staphylococcus aureus protein A (SpA) in HBS buffer (10 mM HEPES, 150 mM NaCl, 0.005% surfactant Tween 20) was injected, followed by incubation at room temperature for 2 hours. Finally, the blocking was performed using 10 mg·mL^{-1} bovine serum albumin (BSA) in HBS for 1 hour.

In the functionalization for IgG detection using ZZ-BNC, after cleaning the QCM by injecting piranha solution and rinsing with ultrapure water, we injected the 80 μg·mL^{-1} ZZ-BNC in HBS buffer and incubated overnight. Then, the 10 mg·mL^{-1} BSA in HBS buffer was injected for blocking.

MEMS QCM Functionalization for CRP Detection

For the CPR detection using ZZ-BNC, the 80 μg·mL^{-1} ZZ-BNC in HBS buffer was injected after activating the SAM molecules. The sensor chip was then incubated for 2 hours. Subsequently, the 200 μg·mL^{-1} anti-CRP antibody in HBS for capturing the CRP was injected, followed by incubation at room temperature for 2 hours. After BSA blocking, the sensor chip was washed using an HBS buffer.

Measurement System

After functionalization, the MEMS QCM biosensor chip was set in the homebuilt sensor cell. The frequency response of the QCM was monitored by connecting the conductive layers on the lower and upper glass substrates to a vector network analyzer (ZNLE3, Rohde & Schwarz) using needle contact probes. The IgG and CRP with various concentrations in HBS buffer were injected into the MEMS QCM biosensor using a micropump at a flow rate of 150 μL·min^{-1}. The IgG detection measurement was performed at room temperature. The IgG molecules were dissociated from protein A after one measurement by flowing glycine-HCl buffer (GHB, 50mM, pH2.2), and the sensor chip was reused. The CRP detection was performed at 37 °C by keeping the analyte solution inside a water bath.

Chemicals and Proteins

10-carboxy-decanthiol (#C385), EDC (#W001) and HEPES (#346-01373) were obtained from DOJINDO. Protein A (#101100) was from Invitrogen. BSA (#A3059) was from Sigma

Aldrich. NHS (#087-09371), rIgG (#148-09551) and GHB (#077-04711) were from Wako. CRP (#8C72) and anti-CRP antibody (#4C28cc-C2cc) were from HyTest Ltd.

RESULTS AND DISCUSSION

Structure of the MEMS QCM

The structure of each MEMS QCM sensor chip is shown in Fig. 1. The thickness of the bonding Si layer and the height of the microchannel are 20 μm and 10 μm, respectively. The thickness of the QCM is 13.5 μm or 10 μm, corresponding to the fundamental through-thickness shear resonance of 125 MHz or 166 MHz, respectively.

Since quartz crystal is a piezoelectric material, its mechanical vibration can be excited by a dynamic electric field without any contacts. A continuous signal sent to one of the inner antennas generates an alternating electric field mainly along the thickness direction of the quartz resonator, which excites the shear oscillation of the resonator through the converse piezoelectric effect. The mechanical vibration of the resonator radiates the electric field because of the piezoelectric effect, which is detected by the other antenna. A frequency sweep then determines the mechanical resonant frequency of the quartz resonator.

The single chip has a size of $6\times6\times1$ mm^3. Because of the reduced distance between the QCM and the antenna, the signal intensity is significantly improved by a factor of ~ 100, and even a power instrument as low as a few milliwatts can be used for the operation. The shortened microchannel also greatly reduces the required volume of functionalization reagents and analyte samples in bioassay. The yield rate of the chip fabrication is currently around 70% or less at the lab level, but further improvement of the yield rate is expected by improving the MEMS process environment. The difference in sensitivity between successfully fabricated chips is small. For example, three repeated measurements in Fig. 2C, Fig. 3C, and Fig. 4B were performed using different sensor chips: The reproducible frequency responses indicate nearly identical performance of the fabricated sensor chips.

The resonant frequency of a QCM biosensor is generally affected by both the addition of target mass and viscosity changes at the sensor surface. However, the higher the fundamental frequency of QCM, the smaller the frequency change due to the viscosity effect compared to the mass loading effect,[20] although the former cannot be ignored completely.

IgG Detection using Protein A Functionalized MEMS QCM Biosensor

Figure 2A illustrates the functionalization process of the MEMS QCM biosensor, where the reagent solutions are injected into the sensor chip through a pipette tip. Because the quartz resonator is embedded in the microchannel, we are able to complete the functionalization process with a tiny amount of reagent solutions ($\sim$5 μL). Figure 2B shows the QCM surface after functionalization and during IgG detection. The frequency responses of the MEMS QCM biosensor during the binding reaction between protein A and IgG in three repeated measurements are shown in Fig. 2C. We performed the detection of IgG with various concentrations from 0 to 100 ng·mL^{-1} using the 125-MHz MEMS QCM. The measurement results indicate a detection limit of 1 ng·mL^{-1} or less. Figure S2 shows a long-term measurement for the IgG detection. The frequency returns to the original baseline after the continues measurements of 12 hours and no frequency drift along with time was observed during the measurement, indicating the good reusability and frequency stability of the MEMS QCM. Because of the random orientation of the immobilized protein A, the area density of the effective binding site is limited. Therefore a long reaction time is needed ($\sim$1 hour) until a significant decrease in frequency can be observed in the detection of low-concentration IgG as shown in the inset of Fig. 2C.

Response Enhanced MEMS QCM by ZZ-BNC

We then enhance the frequency response of the MEMS QCM biosensor by increasing the effective binding sites to detection targets through the ZZ-BNC. The ZZ-BNC was synthesized according to the procedures developed in the previous studies.[44,48] Figure 3A illustrates the structure of the ZZ-BNC, which is composed of approximately 120 transmembrane N-terminally ZZ-fused L (ZZ-L) proteins embedded in the lipid bilayer. Figure 3B illustrates the QCM surface functionalized by ZZ-BNC for IgG detection. The ZZ-BNC with the protein A derived ZZ-L proteins for binding IgG has a diameter of ∼32 nm.[46] A single ZZ-BNC is expected to bind ∼60 IgG molecules with their Fab regions orienting outwardly.[48] Figure 3C shows frequency responses on the IgG detection using the 125-MHz antenna-embedded MEMS QCM biosensor with ZZ-BNCs. Figure 3D compares the amount of the frequency decrease at 30 min from the injection with and without ZZ-BNCs. The significantly larger frequency change with ZZ-BNC than that with only protein A confirms the effectiveness of the ZZ-BNC in enhancing the QCM response.

The frequency response of QCM during the binding reaction between immobilized receptors and targets injected in a flow-injection system can be described as,[50,51]

$$\frac{\Delta f(t)}{f_0} = A \cdot \left(e^{-\alpha \cdot t} - 1\right), \tag{1}$$

with the exponential coefficient $\alpha = k_a C_A + k_d$, where the C_A denotes the target concentration in the flowing solution, and k_a and k_d are the reaction velocity constants for association and dissociation, respectively. The fitting to the results in Figs. 2C and 3C give the exponential coefficients as shown in Fig. 3E as a function of the IgG concentration. We calculated the binding affinity, $K_A = k_a/k_d$, between IgG and the protein A and between IgG and ZZ-BNC: It is 0.64×10^9 M^{-1} for the former and 1.47×10^9 M^{-1} for the latter as shown in the inset of Fig. 3E. The larger affinity between IgG and ZZ-BNC indicates that the response enhancement of the MEMS QCM biosensor can be attributed not only to the more effective

binding sites but also to the enhancement of the binding affinity.

One may doubt the validity of Eq.(1) because the tungsten pillars affect the shear flow of the solution. Although it is difficult to quantify this effect, it would be insignificant because the quartz resonator is not connected to the pillars rigidly and the diameter of the pillar (100 μm) is much smaller than that of the resonator (1.5 mm) . In fact, the affinity value determined here for the binding of protein A to IgG is comparable to that reported in previous study without using the pillars,[19] suggesting that Eq. (1) is applicable.

CRP Detection using ZZ-BNC Functionalized MEMS QCM

Using the MEMS QCM biosensor in combination with the ZZ-BNC, we then detected CRP, which is an essential biomarker of infection and inflammation.[52,53] Because the QCM biosensor with a higher frequency shows a better sensitivity, we used 166-MHz MEMS-QCM sensor chips for the CRP detection. In the IgG detection, the ZZ-BNC was directly immobilized on the QCM surface through the Au-S covalent linkages.[43] When functionalizing the MEMS QCM for CRP detection, we used SAM to immobilize the ZZ-BNC on the QCM surface strongly. After the blocking procedure, the anti-CRP antibody was injected to immobilize them on the ZZ-BNCs as shown in Fig. 4A. Such binding sites with a three-dimensional architecture can increase the binding area and alleviate the steric-hindrance effect, thus, is expected to further increase the sensitivity of the CRP detection. Figure 4B shows the frequency responses of the 166-MHz MEMS QCM biosensor during the CRP solution flow. The results indicate a detection limit of 1 ng·mL^{-1} or less.

The optimal response time can be determined as the shortest time at which a reliable difference in the amount of frequency reduction is observed. For example, although the CRP detection result was obtained within one hour, the actual measurement time can be reduced to about 10 min as shown in Figure 4C, where the amount of frequency decrease after 10 min correlates linearly with the logarithm of the CRP concentration. The signal intensity of the fabricated sensor chip varies to some extent in the current lab-level manufacturing process,

but the frequency response to the captured target is nearly identical. This is because the mass sensitivity of QCM is essentially determined by the fundamental resonant frequency, or the thickness of the quartz resonator, and in the MEMS-QCMs, the variation in the resonator thickness is very small (<∼2%). Therefore, the calibration results from randomly selected sensor chips apply to other successfully fabricated chips because of the good sensitivity uniformity.

Table I compares the CRP detection sensitivity of this work with those of reported methods. The sensitivity for CRP detection using the MEMS QCM and the ZZ-BNC in this work is comparable to or much better than the previous methods, demonstrating the promising application of developed MEMS QCM in highly sensitive bioassay.

Table 1: Sensitivity comparison of various biosensor methods in CRP detection

Method	Detection materials	Detection limit	Ref.
Sandwich ELISA	Capture anti-CRP/CRP/detection anti-CRP	1 ng·mL^{-1}	[54]
Sandwich ELISA	Anti-CRP bound Dynabeads/CRP/anti-CRP	0.4 ng·mL^{-1}	[55]
EIS[a]	Anti-CRP immobilized on carbon nanofibers	11 ng·mL^{-1}	[56]
EIS	Anti-CRP on AuNPs-modified graphene	15 ng·mL^{-1}	[57]
ECS[b]	Anti-CRP on polyaniline films	500 ng·mL^{-1}	[58]
SPR	Anti-CRP on gold surface	9 ng·mL^{-1}	[59]
SPR	Biotinylated CRP aptamer	5 ng·mL^{-1}	[60]
SPR	Oriented anti-CRP through protein A/G	1.2 ng·mL^{-1}	[61]
QCM (5 MHz)	Oriented anti-CRP through protein A	3 μg·mL^{-1}	[21]
QCM (6 MHz)	Anti-CRP/CRP/AuNP-conjugated anti-CRP	20 ng·mL^{-1}	[62]
QCM (20 MHz)	Anti-CRP/CRP/anti-CRP/AuNPs	20 ng·mL^{-1}	[63]
This work	Oriented anti-CRP through ZZ-BNC	1 ng·mL^{-1}	

[a] Electrochemical impedance spectroscopy; [b] Electrochemical capacitance spectroscopy.

CONCLUSIONS

In this work, we presented a wafer-scale mass-fabrication MEMS process for obtaining many ultra-sensitive QCM biosensors, where the antennas are formed inside the microchannel. The short distance (∼10 μm) between the antennas and the quartz resonator extends the operation frequency higher than 160 MHz. Compared to conventional QCMs with fundamental

resonant frequencies of 10 MHz or lower, the high-frequency MEMS QCM developed here significantly improves the detection sensitivity of biomarkers. In addition, it can be available at a low cost because of the mass production. Furthermore, the microfluidic channel in the sensor chip effectively decreases the consumption of reagents and analyte samples.

We applied this sensor chip to the IgG detection. Much larger frequency change was observed when ZZ-BNCs were immobilized on the QCM surface, and the binding affinity was also improved with ZZ-BNC, achieving the detection limit of 1 ng·mL^{-1} or less despite the direct assay. We then applied the 166-MHz MEMS-QCM chip for detecting CRP and also confirmed high sensitivity with the detection limit of 1 ng·mL^{-1} or less. Thus, the wireless MEMS-QCM biosensors developed with the fabrication process proposed in this work have the advantages of compact size, low cost, low-power consumption, and high sensitivity.

ASSOCIATED CONTENT

Supporting Information

Wafer-level fabrication process of MEMS QCM (Figure S1) and long-term measurement of IgG detection (Figure S2) (PDF)

AUTHOR INFORMATION

Corresponding Authors

*E-mail ogi@prec.eng.osaka-u.ac.jp (H.O.).

Author Contributions

L.Z. performed the QCM measurements, analyzed data, and wrote the paper. F.K. proposed the MEMS process and fabricated the MEMS QCM. L.Z. and F.K. equally contributed

to this study. S.K. and M.I developed the ZZ-BNC. T.N. fabricated the MEMS QCM. H.O. (corresponding author) promoted this study, fabricated the MEMS QCM, analyzed the results, and wrote the paper.

ACKNOWLEDGMENTS

This research was partially supported by JSPS KAKENHI Grant (No. 19H00862) and Development of Advanced Measurement and Analysis Systems from Japan Science and Technology Agency (No. JP-MJSN16B5).

References

(1) Bhalla, N.; Jolly, P.; Formisano, N.; Estrela, P. *Essays Biochem.* **2016**, *60*, 1–8.

(2) Udugama, B.; Kadhiresan, P.; Kozlowski, H. N.; Malekjahani, A.; Osborne, M.; Li, V. Y.; Chen, H.; Mubareka, S.; Gubbay, J. B.; Chan, W. C. *ACS nano* **2020**, *14*, 3822–3835.

(3) Kevadiya, B. D. et al. *Nat. Mater.* **2021**, *20*, 593–605.

(4) Masterson, A. N.; Muhoberac, B. B.; Gopinadhan, A.; Wilde, D. J.; Deiss, F. T.; John, C. C.; Sardar, R. *Anal. Chem.* **2021**, *93*, 8754–8763.

(5) Homola, J. *Anal. Bioanal. Chem.* **2003**, *377*, 528–539.

(6) Wang, J.; Zhou, H. S. *Anal. Chem.* **2008**, *80*, 7174–7178.

(7) Piliarik, M.; Bocková, M.; Homola, J. *Biosens. Bioelectron.* **2010**, *26*, 1656–1661.

(8) Qu, J. H.; Dillen, A.; Saeys, W.; Lammertyn, J.; Spasic, D. *Anal. Chim. Acta* **2020**, *1104*, 10–27.

(9) Watanabe, S.; Murozaki, Y.; Sugiura, H.; Sato, Y.; Honbe, K.; Arai, F. *Sens. Actuators A: Phys.* **2021**, *317*, 112475.

(10) Chappanda, K. N.; Shekhah, O.; Yassine, O.; Patole, S. P.; Eddaoudi, M.; Salama, K. N. *Sens. Actuators B: Chem.* **2018**, *257*, 609–619.

(11) Yao, Y.; Huang, X.; Zhang, B.; Zhang, Z.; Hou, D.; Zhou, Z. *Sens. Actuators B: Chem.* **2020**, *302*, 127192.

(12) Jin, X.; Huang, Y.; Mason, A.; Zeng, X. *Anal. Chem.* **2009**, *81*, 595–603.

(13) Rianjanu, A.; Fauzi, F.; Triyana, K.; Wasisto, H. S. *ACS Appl. Nano Mater.* **2021**, *4*, 9957–9975.

(14) Zhou, L.; Nakamura, N.; Nagakubo, A.; Ogi, H. *Appl. Phys. Lett.* **2019**, *115*, 171901.

(15) Chen, D.; Li, H.; Su, X.; Li, N.; Wang, Y.; Stevenson, A. C.; Hu, R.; Li, G. *Sens. Actuators B: Chem.* **2019**, *287*, 35–41.

(16) Reviakine, I.; Johannsmann, D.; Richter, R. P. *Anal. Chem.* **2011**, *83*, 8838–8848.

(17) Ogi, H. *Proc. Jpn. Acad., Ser. B, Phys. Biol. Sci.* **2013**, *89*, 401–417.

(18) Sauerbrey, G. *Z. Phys.* **1959**, *55*, 206–222.

(19) Ogi, H.; Fukunishi, Y.; Omori, T.; Hatanaka, K.; Hirao, M.; Nishiyama, M. *Anal. Chem.* **2008**, *80*, 5494–5500.

(20) Ogi, H.; Nagai, H.; Fukunishi, Y.; Hirao, M.; Nishiyama, M. *Anal. Chem.* **2009**, *81*, 8068–8073.

(21) Zhang, Y.; Rojas, O. J. *Biomacromolecules* **2017**, *18*, 526–534.

(22) Hampitak, P.; Jowitt, T. A.; Melendrez, D.; Fresquet, M.; Hamilton, P.; Iliut, M.; Nie, K.; Spencer, B.; Lennon, R.; Vijayaraghavan, A. *ACS Sens.* **2020**, *5*, 3520–3532.

(23) Hu, J.; Yesilbas, G.; Li, Y.; Geng, X.; Li, P.; Chen, J.; Wu, X.; Knoll, A.; Ren, T. L. *Anal. Chem.* **2022**, *94*, 5760–5768.

(24) Kato, F.; Ogi, H.; Yanagida, T.; Nishikawa, S.; Hirao, M.; Nishiyama, M. *Biosens. Bioelectron.* **2012**, *33*, 139–145.

(25) Kato, F.; Noguchi, H.; Kodaka, Y.; Oshida, N.; Ogi, H. *Jpn. J. Appl. Phys.* **2018**, *57*, 07LD14.

(26) Zhou, L.; Kato, F.; Ogi, H. *Jpn. J. Appl. Phys.* **2021**, *60*, SDDB03.

(27) Noi, K.; Iwata, A.; Kato, F.; Ogi, H. *Anal. Chem.* **2019**, *91*, 9398–9402.

(28) Jiang, X.; Wang, R.; Wang, Y.; Su, X.; Ying, Y.; Wang, J.; Li, Y. *Biosens. Bioelectron.* **2011**, *29*, 23–28.

(29) Chen, Q.; Tang, W.; Wang, D.; Wu, X.; Li, N.; Liu, F. *Biosens. Bioelectron.* **2010**, *26*, 575–579.

(30) Dong, Z. M.; Jin, X.; Zhao, G. C. *Biosens. Bioelectron.* **2018**, *106*, 111–116.

(31) Yang, H.; Li, Y.; Wang, D.; Liu, Y.; Wei, W.; Zhang, Y.; Liu, S.; Li, P. *ChemComm.* **2019**, *55*, 5994–5997.

(32) Ogi, H.; Yanagida, T.; Hirao, M.; Nishiyama, M. *Biosens. Bioelectron.* **2011**, *26*, 4819–4822.

(33) Thies, J. W.; Kuhn, P.; Thürmann, B.; Dübel, S.; Dietzel, A. *Microelectron. Eng.* **2017**, *179*, 25–30.

(34) Noi, K.; Iijima, M.; Kuroda, S.; Ogi, H. *Sens. Actuators B: Chem.* **2019**, *293*, 59–62.

(35) Lee, D.; Yoo, M.; Seo, H.; Tak, Y.; Kim, W. G.; Yong, K.; Rhee, S. W.; Jeon, S. *Sens. Actuators B: Chem.* **2009**, *135*, 444–448.

(36) Yan, J.; Zhao, C.; Ma, Y.; Yang, W. *Biomacromolecules* **2022**, *23*, 2614–2623.

(37) Liu, Y.; Yu, J. *Microchim. Acta* **2016**, *183*, 1–19.

(38) Park, M. *Biochip J.* **2019**, *13*, 82–94.

(39) Yuan, Y.; He, H.; Lee, L. J. *Biotechnol. Bioeng.* **2009**, *102*, 891–901.

(40) Tajima, N.; Takai, M.; Ishihara, K. *Anal. Chem.* **2011**, *83*, 1969–1976.

(41) Neubert, H.; Jacoby, E. S.; Bansal, S. S.; Iles, R. K.; Cowan, D. A.; Kicman, A. T. *Anal. Chem.* **2002**, *74*, 3677–3683.

(42) Kausaite-Minkstimiene, A.; Ramanaviciene, A.; Kirlyte, J.; Ramanavicius, A. *Anal. Chem.* **2010**, *82*, 6401–6408.

(43) Iijima, M.; Nakayama, T.; Kuroda, S. *Biosens. Bioelectron.* **2020**, *150*, 111860.

(44) Iijima, M.; Matsuzaki, T.; Kadoya, H.; Hatahira, S.; Hiramatsu, S.; Jung, G.; Tanizawa, K.; Kuroda, S. *Anal. Biochem.* **2010**, *396*, 257–261.

(45) Nilsson, B.; Moks, T.; Jansson, B.; Abrahmsen, L.; Elmblad, A.; Holmgren, E.; Henrichson, C.; Jones, T. A.; Uhlén, M. *Prot. Eng.* **1987**, *1*, 107–113.

(46) Iijima, M.; Somiya, M.; Yoshimoto, N.; Niimi, T.; Kuroda, S. *Sci. Rep.* **2012**, *2*, 00790.

(47) Noi, K.; Iijima, M.; Kuroda, S.; Kato, F.; Ogi, H. *Jpn. J. Appl. Phys.* **2020**, *59*, SKKB03.

(48) Iijima, M. et al. *Biomaterials* **2011**, *32*, 1455–1464.

(49) Kato, F.; Ogi, H.; Yanagida, T.; Nishikawa, S.; Nishiyama, M.; Hirao, M. *Jpn. J. Appl. Phys.* **2011**, *50*, 07HD03.

(50) Liu, Y.; Yu, X.; Zhao, R.; Shangguan, D. H.; Bo, Z.; Liu, G. *Biosens. Bioelectron.* **2003**, *19*, 9–19.

(51) Ogi, H.; Motohisa, K.; Hatanaka, K.; Ohmori, T.; Hirao, M.; Nishiyama, M. *Biosens. Bioelectron.* **2007**, *22*, 3238–3242.

(52) Christodoulides, N.; Mohanty, S.; Miller, C. S.; Langub, M. C.; Floriano, P. N.; Dharshan, P.; Ali, M. F.; Bernard, B.; Romanovicz, D.; Anslyn, E.; Fox, P. C.; McDevitt, J. T. *Lab Chip* **2005**, *5*, 261–269.

(53) Vashist, S. K.; Venkatesh, A. G.; Schneider, E. M.; Beaudoin, C.; Luppa, P. B.; Luong, J. H. *Biotechnol. Adv.* **2016**, *34*, 272–290.

(54) Zhang, L.; Li, H. Y.; Li, W.; Shen, Z. Y.; Wang, Y. D.; Ji, S. R.; Wu, Y. *Front. immunol.* **2018**, *9*, 1–5.

(55) Vashist, S. K.; Czilwik, G.; Oordt, T. V.; Stetten, F. V.; Zengerle, R.; Schneider, E. M.; Luong, J. H. *Anal. Biochem.* **2014**, *456*, 32–37.

(56) Gupta, R. K.; Periyakaruppan, A.; Meyyappan, M.; Koehne, J. E. *Biotechnol. Bioeng.* **2014**, *59*, 112–119.

(57) Boonkaew, S.; Chaiyo, S.; Jampasa, S.; Rengpipat, S.; Siangproh, W.; Chailapakul, O. *Microchim. Acta* **2019**, *186*, 1–10.

(58) Baradoke, A.; Hein, R.; Li, X.; Davis, J. J. *Anal. Chem.* **2020**, *92*, 3508–3511.

(59) Aray, A.; Chiavaioli, F.; Arjmand, M.; Trono, C.; Tombelli, S.; Giannetti, A.; Cennamo, N.; Soltanolkotabi, M.; Zeni, L.; Baldini, F. *J. Biophotonics* **2016**, *9*, 1077–1084.

(60) Bini, A.; Centi, S.; Tombelli, S.; Minunni, M.; Mascini, M. *Anal. Bioanal. Chem.* **2008**, *390*, 1077–1086.

(61) Vashist, S. K.; Schneider, E. M.; Luong, J. H. *Analyst* **2015**, *140*, 4445–4452.

(62) Ding, P.; Liu, R.; Liu, S.; Mao, X.; Hu, R.; Li, G. *Sens. Actuators B: Chem.* **2013**, *188*, 1277–1283.

(63) Gao, K.; Cui, S.; Liu, S. *Int. J. Electrochem. Sci.* **2018**, *13*, 812–821.

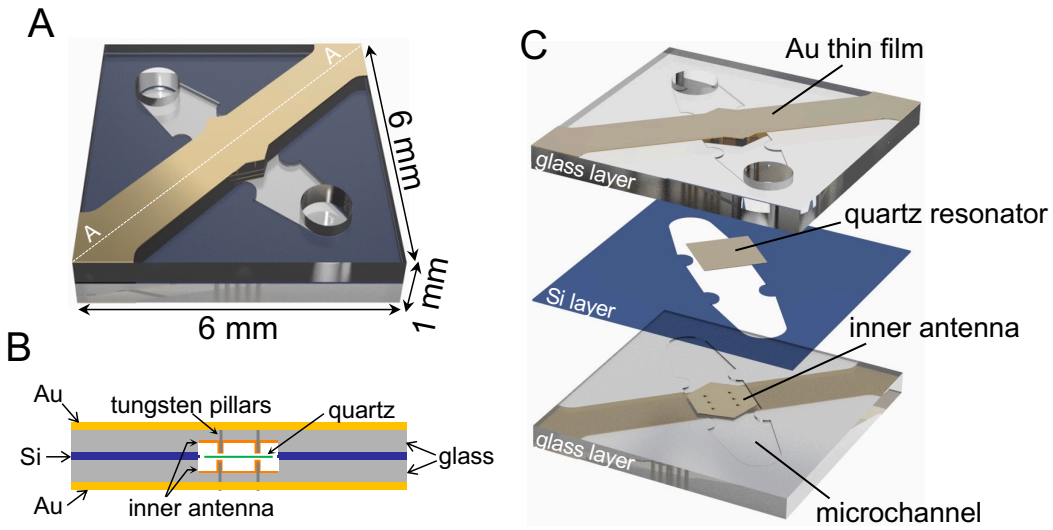

Figure 1: (A) Illustration of the fabricated MEMS QCM biosensor chip and (B) its cross-section view. (C) Explanation of the three-layer structure of the chip.

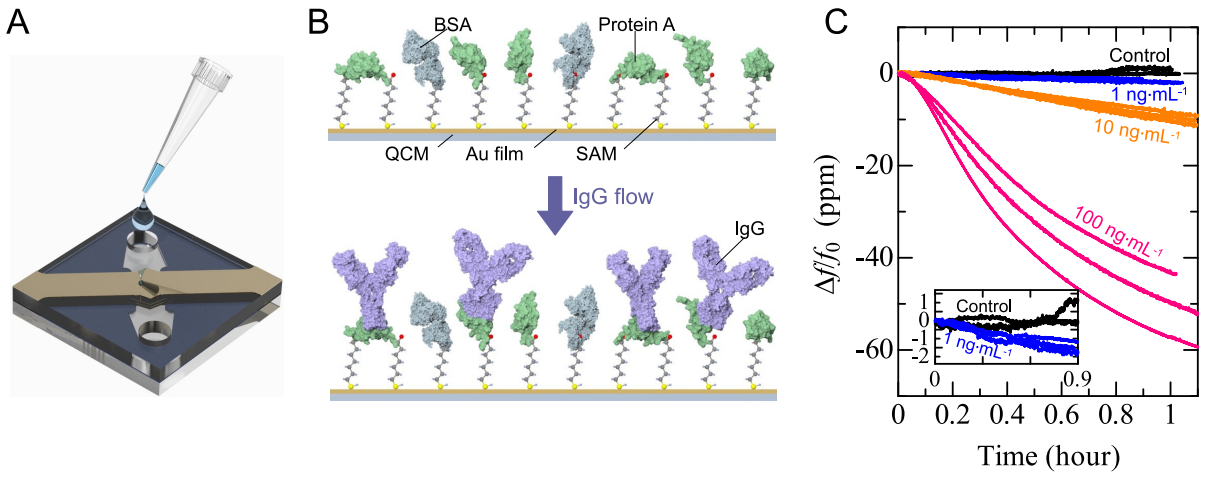

Figure 2: (A) Illustration of the MEMS QCM functionalization process. (B) Schematic of the QCM surface functionalized by SAM and protein A for IgG detection. (C) Frequency responses of the 125-MHz MEMS QCM biosensor in IgG detection during the binding reaction.

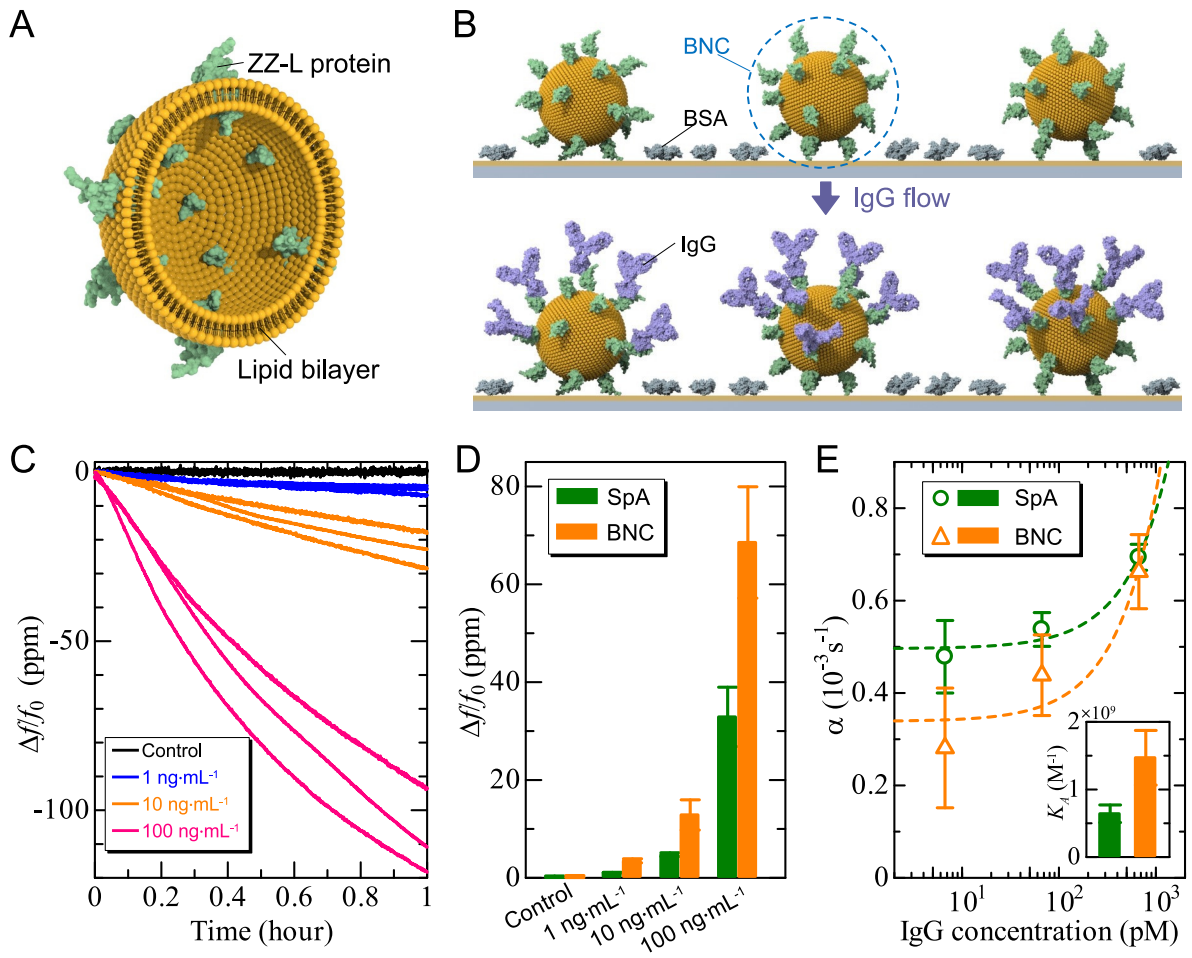

Figure 3: (A) Illustration of the cross-section of the ZZ-BNC. (B) Schematic of the QCM surface functionalized by ZZ-BNC for IgG detection. (C) Frequency responses of the 125-MHz MEMS QCM biosensor in IgG detection during the binding reaction. (D) Frequency decreases measured by the 125-MHz MEMS QCM in IgG detection using protein A and ZZ-BNC at 30 min. (E) Exponential coefficients of the frequency decrease curves in IgG detection using protein A and ZZ-BNC as functions of the IgG concentration. The inset shows the binding affinity between IgG and protein A and between IgG and ZZ-BNC.

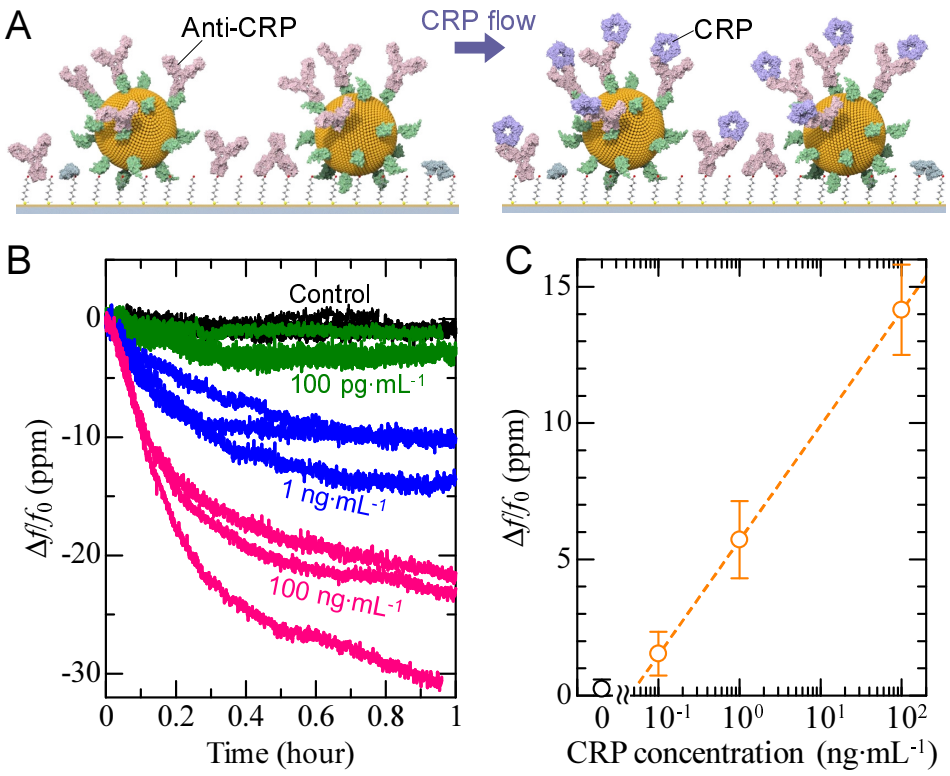

Figure 4: (A) Schematic of the QCM surface functionalized by ZZ-BNC and anti-CRP antibody for CRP detection. (B) Frequency responses of the 166-MHz MEMS QCM biosensor in CRP detection during the binding reaction. (C) Frequency decreases at 10 min against the logarithm of CRP concentration.

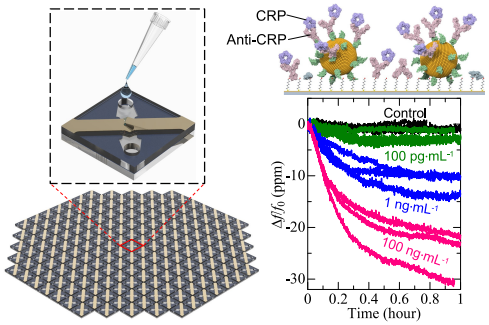

For Table of Contents Only

Mass-fabrication scheme of highly sensitive wireless electrodeless MEMS QCM biosensor with antennas on inner walls of microchannel

Lianjie Zhou,[†,⊥] Fumihito Kato,[‡,⊥] Masumi Iijima,[¶] Tomoyuki Nonaka,[§] Shun'ichi Kuroda,[‖] and Hirotsugu Ogi[*,†]

†Graduate School of Engineering, Osaka University, Yamadaoka 2-1, Suita, Osaka 565-0871, Japan
‡Department of Mechanical Engineering, Nippon Institute of Technology, Gakuendai 4-1, Miyashiro-machi, Minamisaitama, Saitama 345-8501, Japan
¶Department of Nutritional Science and Food Safety, Tokyo University of Agriculture, Sakuragaoka 1-1-1, Setagaya-ku, Tokyo 156-8502, Japan
§Samco Inc., Waraya-cho 36, Takeda, Fushimi-ku, Kyoto 612-8443, Japan
‖The Institute of Scientific and Industrial Research, Osaka University, Mihogaoka 8-1, Ibaraki, Osaka 567-0047, Japan
⊥Contributed equally to this work

*E-mail: ogi@prec.eng.osaka-u.ac.jp

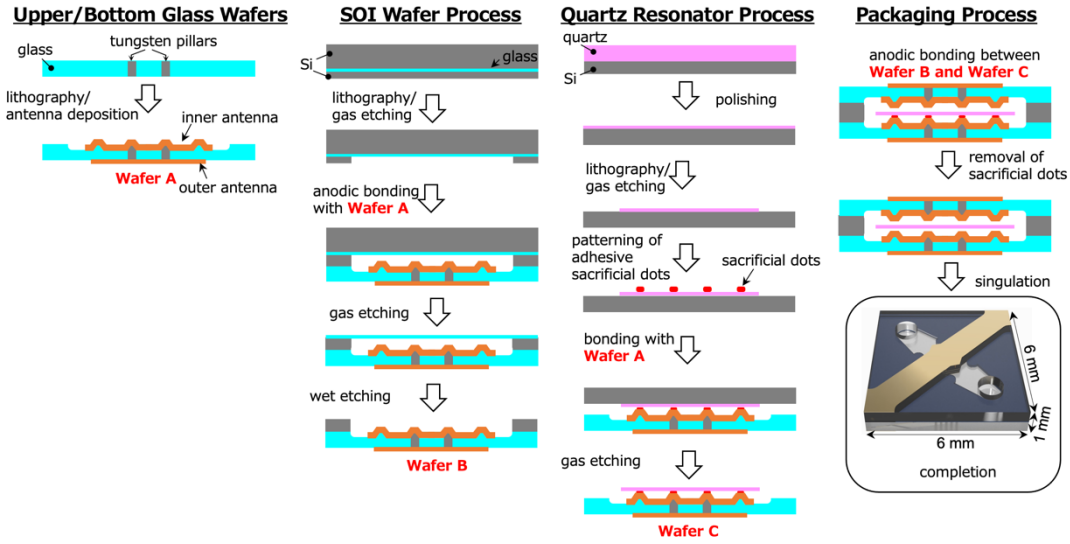

Figure S1 4-inch wafer-level MEMS process for fabricating ~180 ultra-high sensitive QCM biosensors. This MEMS process consists of four processes: (i) Glass-wafer process for fabricating upper and bottom glass wafers with microchannels and inner and outer antennas, (ii) silicon-on-insulator (SOI) wafer process for making the middle Si layer as the bonding layer, (iii) quartz-wafer process for patterning the isolated thin quartz resonators, and (iv) packaging process.

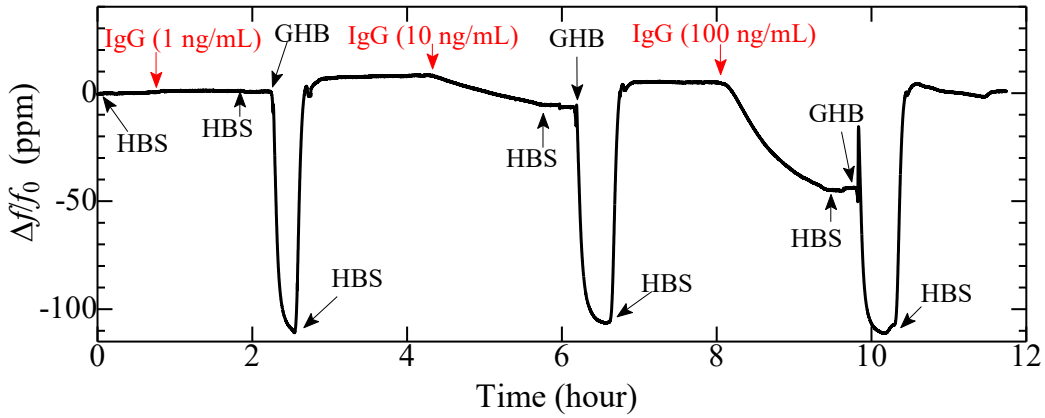

Figure S2 Frequency response of a 125 MHz MEMS QCM in a long-term measurement of IgG detection.